A patchwork (back)projector to accelerate artifact reduction in CT reconstruction

Katrien Van Slambrouck and Johan Nuyts

***Abstract*—Artifacts in computed tomography (CT) reconstruction are often caused by an inaccurate modeling of the acquisition during reconstruction. These artifacts can be severe when metals are in the field of view. A better modeling of the acquisition during reconstruction reduces artifacts but often leads to a substantial increase in computation time. Because metals are the most prominent source of the artifacts, we hypothesize it would be sufficient to limit the more complex model to regions close to metals and use less complex, faster models for the other parts. For this purpose we present a patchwork (back)projector, embedded in an iterative reconstruction algorithm, which is able to change reconstruction properties for a particular area in the object. We combined reconstruction models with different complexity for the reduction of non-linear partial volume effects and beam hardening. In this way we reduced the computation time while keeping the same image quality. Moreover, an improved convergence is achieved by dividing the image into subareas, patches. The presented results are for a two dimensional geometry, in the future we will extend this to three dimensions.**

I. Introduction

Classic computed tomography (CT) reconstruction often suffers from severe artifacts when metallic objects are in the field-of-view. These artifacts are mostly caused by a discrepancy between the true acquisition process and the model used during reconstruction [1]. Consequently, most artifacts can be reduced by using a more accurate acquisition model in the reconstruction. Unfortunately, algorithms which use a more accurate acquisition model need much more computation time.

We hypothesize that we can limit the more accurate but complex modeling of the acquisition to areas in the object that contain metals, because metals are often the most prominent source of the artifacts. A less complex, faster model can then be used for the rest of the object.

In this work we will consider two important causes of (metal) artifacts: non-linear partial volume effects and beam hardening.

The nonlinear partial volume effect is mainly important near edges between different materials. It stems from averaging the attenuation coefficient over the in-plane and axial width of the focal spot and the detector elements. Most algorithms (implicitly) assume that partial volume effects result in a linear combination of the attenuation values. However, the true process is non-linear and varies with the angle of the projection line. It is shown that reconstruction on a finer grid [2] reduces artifacts. Likewise, a denser sampling of the detector elements and/or the focal spot is expected to reduce artifacts.

Dept. of Nuclear Medicine, K.U.Leuven, B-3000 Leuven, Belgium. katrien.vanslambrouck@uz.kuleuven.be. This work is supported by the SBO-project QUANTIVIAM (060819) of the Institute for the Promotion of Innovation through Science and Technology in Flanders (IWT-Vlaanderen) and a 2010 IEEE NSS-MIC Trainee Grant.

Beam hardening artifacts are due to the polychromatic nature of the x-ray beams. This causes severe artifacts especially when metals are present in the object. Statistical iterative reconstruction with polychromatic model is an important way to reduce beam hardening artifacts caused by metals [3][4][5]. In principle, statistical iterative reconstruction with polychromatic model is superior to projection completion methods [6][7][8], because projection completion destroys potentially useful information about the metal itself and its surroundings.

In section II we present our patchwork projector and the patchwork reconstruction structure that combines different resolution and projection models depending on the location in the object. Section III presents the experiments we performed. The results are shown in section IV. The description and experiments are presented for a 2D fan beam geometry. Extensions to other geometries are possible.

II. Methods

A. The patchwork (back)projector

The goal is to develop a reconstruction structure with different projection properties depending on the particular location in the reconstruction volume. The projection structure will be called the patchwork projector and can be introduced in an iterative reconstruction algorithm. We divide the reconstruction volume into areas or *patches*. Subsequently, we can adjust the projection properties for each of the different patches. Our patchwork projector is based on a distance driven projector [9].

The patches are updated sequentially in each iteration, i.e. each patch is treated as a separate group in a grouped coordinate ascent algorithm as in [10]. The sequential update and the smaller field of view for smaller patches can result in an increased convergence, as also described in [10].

B. Reconstruction

Reconstruction was done by using filtered backprojection (FBP), maximum likelihood for transmission (MLTR) [11], a polychromatic modification to MLTR (MLTR_C) and iterative maximum likelihood polychromatic algorithm for CT (IMPACT) [3].

MLTR, MLTR_C, and IMPACT are maximum likelihood algorithms based on the Poisson likelihood L:

$$L = \sum_{i}^{I} \left(y_i \ln \hat{y}_i - \hat{y}_i \right) \tag{1}$$

with i the index of the projection lines, I the total number of projection lines, y_i the measured transmission scan and $\hat{y}_i$

the estimated transmission scan. The following update step is applied [11]:

$$\mu_j^{\text{new}} = \mu_j^{\text{old}} + \frac{\frac{\partial L}{\partial \mu_j}\Big|_{\vec{\mu}^{\text{old}}}}{\sum_h^J \frac{\partial^2 L}{\partial \mu_j \partial \mu_h}\Big|_{\vec{\mu}^{\text{old}}}} \tag{2}$$

The different reconstruction algorithms use a different basic projection model which is explained in the following.

1) MLTR: MLTR has a regular monochromatic projection model for transmission:

$$\hat{y}_i = b_i \exp\big(-\sum_j^J l_{ij}\mu_j\big) \tag{3}$$

with i the index of the projection lines, j the pixel index, J the total number of pixels, b_i the blank value for projection line i, l_{ij} the intersection length of projection line i and pixel j and μ_j the linear attenuation in pixel j.

2) MLTR_C: MLTR_C is based on MLTR but takes into account the polychromatic behavior of water via a simple water correction, the projection model becomes:

$$\hat{y}_i = \sum_k^K b_{ik} \exp\big(-P_k \sum_j^J l_{ij}\mu_j\big) \tag{4}$$

with k the energy bin, K the total number of bins and b_{ik} the blank value for projection line i at energy k and

$$P_k = \frac{\mu_{\text{ref}}^{\text{water}}}{\mu_k^{\text{water}}} \tag{5}$$

where $\mu_{\text{ref}}^{\text{water}}$ is the linear attenuation for water at a chosen reference energy and μ_k^{water} is the linear attenuation for water at energy k. Note that the complexity (in terms of (back)projections) of this model doesn't change compared to regular MLTR but knowledge about the energy spectrum of the x-ray tube is required.

3) IMPACT: The IMPACT projection model [3] uses a fully polychromatic projection estimate:

$$\hat{y}_i = \sum_k^K b_{ik} \exp\big(-\sum_j^J l_{ij}\mu_{jk}\big) \tag{6}$$

The energy dependent linear attenuation μ_{jk} can be written as a linear combination of the Compton and photo electric component:

$$\mu_{jk} = \Theta_k \theta_j + \Phi_k \phi_j \tag{7}$$

with Θ_k and Φ_k the energy dependence of the Compton scattering and the photoelectric effect respectively and θ_j and ϕ_j the material dependence. We assume that θ_j and ϕ_j are unambiguously determined by the attenuation at a chosen reference energy: $\theta_j = \theta(\mu_{j,\text{ref}})$ and $\phi_j = \phi(\mu_{j,\text{ref}})$. The final projection estimate becomes:

$$\hat{y}_i = \sum_k^K b_{ik} \exp\left(-\Theta_k \sum_j^J l_{ij}\theta(\mu_{j,\text{ref}}) - \Phi_k \sum_j^J l_{ij}\theta(\mu_{j,\text{ref}})\right) \tag{8}$$

When calculating the update step in (2), we can see that the complexity in terms of (back)projections is 8, compared to 3 for MLTR. Again, the energy spectrum of the x-ray tube is required

C. Local models

1) Step 1: Resolution: By increasing the resolution we want to reduce non-linear partial volume artifacts. As said before, these artifacts are prominent around metals. Therefore, we will apply a non-uniform sampling for the different patches. Non uniform grids were already used before [12][13][14] but mainly with a view to increased resolution in regions of interest. Here, the patches containing metals will be reconstructed on a finer grid to limit non-linear partial volume effects at the edges of the metal. Likewise, for the metal patches, the detector elements will be subsampled.

2) Step 2: Reconstruction model: When comparing the complexity of MLTR and IMPACT in terms of (back)projections, we have 3 for MLTR and 8 for IMPACT. We assume that the reduction of beam hardening artifacts in waterlike materials does not need such a complex model and that we can limit IMPACT to patches with metals and other dense objects (e.g. dense bone). Therefore, we will use the IMPACT projection model in the metal and bone patches and a less complex model, MLTR or MLTR_C in the patches containing waterlike materials.

III. Experiments

A. Simulation for the water phantom

Two-dimensional simulations were done by using the CT-simulator created by B. De Man [15], wherein we replaced the ray driven projector by a distance driven projector. The simulator took into account polychromaticity, resolution effects and noise. Resolution effects are introduced via subsampling the detector elements, the view angles (to simulate continuous rotation) and the source (which has a finite width of 0.06 cm) each five times. The pixel size for simulation was 0.05 mm. We simulated a fan-beam geometry with a fan angle of 52.14°, using a flat detector of 101.8 cm with 672 elements and 1160 angles over 360°. We used a water phantom of 18 cm with two (dense) bone inserts (3.2 cm) and two iron inserts (1.2 cm). The phantom is depicted in figure 1(a).

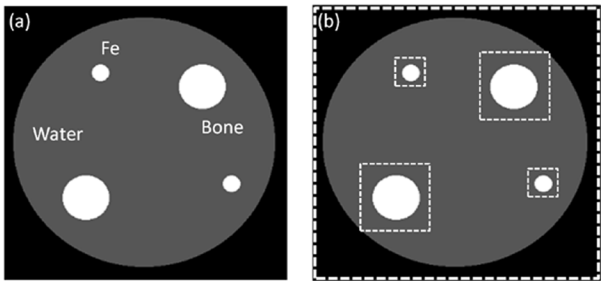

Fig. 1. (a) water phantom with bone and iron inserts, (b) patch structure indicated by dashed lines.

B. Reconstruction

We started by doing a regular FBP, MLTR and IMPACT reconstruction on a 400x400 reconstruction grid, corresponding to an area of 20x20 cm, with a pixel size of 0.5 mm. For the iterative methods we did 50 iterations and used 116 subsets for each iteration.

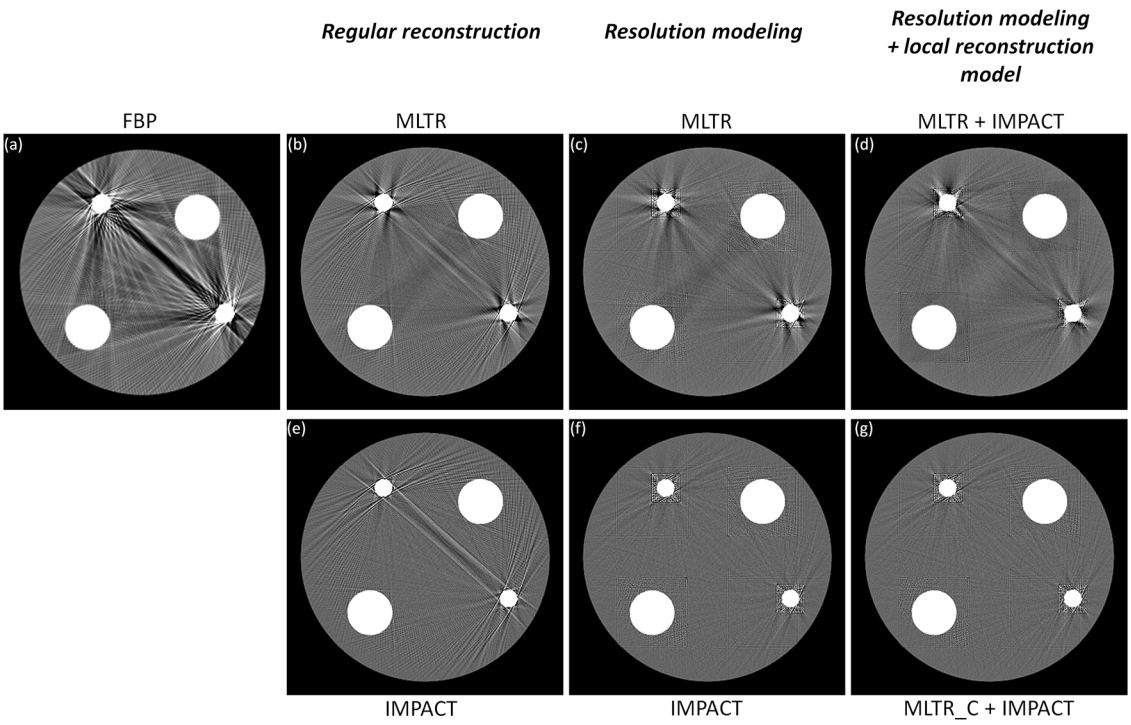

Fig. 2. Reconstructions: reconstruction with FBP (a), reconstruction with regular MLTR (b) and IMPACT (e), reconstruction with patches: increased resolution for iron patch for MLTR (c) and IMPACT (f), reconstruction with patches: increased resolution for iron patch and combination of projection model: MLTR + IMPACT (d), MLTR_C + IMPACT (e). Windowed in interval [-700, 500] HU.

To apply the patchwork reconstruction structure, we have to divide the image into patches. The patchwork structure used for the water phantom is depicted in figure 1(b).

In a first step we increased the resolution for the patches containing iron during the reconstruction. For the iron patches the pixel size was 0.25 mm and they were projected with detector elements which were subsampled twice. The other patches had the regular pixel size (0.5mm) and no detector subsampling. In this first step we used the same projection model for all patches in the image, this was either MLTR or IMPACT.

Finally, we also changed the projection model for the reconstruction. We used the full polychromatic IMPACT model for the iron and bone patches and the MLTR or MLTR_C model for the water patch. The sampling properties are the same as in the previous step.

C. Convergence analysis

To evaluate the influence of the patch structure on the convergence we did the following experiment. We simulated again the fan bean geometry described in III-A to compute the projection of the Shepp-Logan phantom shown in figure 3(a). A noise free monochromatic simulation was done for 800 equally spaced angles over 360°, without any subsampling and with pixel size 0.5 mm. The reconstruction was done using regular MLTR, MLTR for 9 equal patches and MLTR for 25 equal patches. The pixel size (0.5mm) was the same for all three reconstructions and for all patches and no detector subsampling was applied.

To quantify the possible difference in convergence, we calculated the difference between the maximal likelihood and the likelihood for the reconstruction at a certain iteration:

$$\Delta L = L_{\max} - L_{\text{rec}} = \sum_{i}^{I} \Big(y_i(\ln y_i - \ln \hat{y}_i) - (y_i - \hat{y}_i) \Big) \quad (9)$$

We evaluated the convergence for 30 iterations using 5 subsets.

IV. Results

Figure 2 shows the reconstruction for the water phantom. In 2(a) we show the reconstruction with FBP, 2(b) and 2(e) show a regular reconstruction for MLTR and IMPACT respectively. In 2(c) and 2(f) we see the result for the reconstruction with an increased resolution for the pixels and detector elements of the iron patch. All patches are reconstructed with the MLTR (c) or IMPACT (f) projection model. In figure 2(d) and 2(g) we see the result of combining the IMPACT and MLTR or MLTR_C model. IMPACT is used for the iron and bone patch, combined with MLTR (d) and MLTR_C (g) for the water patch. Again the sampling is increased twice for the pixels and the detector elements of the iron patches.

Figure 3 and figure 4 present the result of the convergence analysis. Figure 3 shows the different reconstructions: 3(b) for the regular MLTR reconstruction, 3(c) for an MLTR reconstruction with 9 equally sized patches and 3(d) with 25 equally sized patches. The difference in convergence ΔL is shown in figure 4.

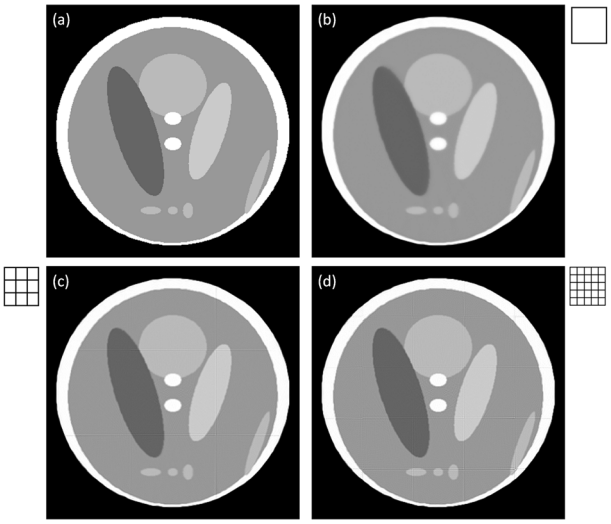

Fig. 3. Convergence analysis, reconstructions: phantom image (a), regular MLTR (b), MLTR with 9 equal patches (c) and MLTR with 25 equal patches. (The patch structure is shown next to the image.)

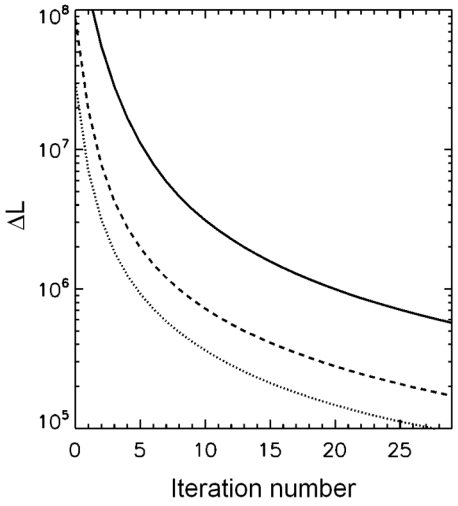

Fig. 4. Convergence analysis, likelihood: ΔL for regular MLTR (solid line), MLTR with 9 patches (dashed line) and MLTR with 25 patches (dotted line).

V. Discussion

We proposed the patchwork reconstruction method which is able to adjust the projection properties depending on the location in the object. For this purpose, we divided the object into subareas, called patches. A different projection model with different resolution can be chosen for each patch.

In a first step we changed the resolution for the patches containing metals. We assumed that a better modeling of non-linear partial volume effects limited to patches containing metals should reduce the artifacts. We increased the sampling both in the reconstruction volume and in the detector. Applying this subsampling to the whole image would dramatically increase the computation time. When comparing the reconstructions (b) with (c), and (e) with (f) in figure 2 we see that streaks originating from the metals are clearly reduced. This is partly because of the better resolution modeling for the metal patches. A second reason is an improved convergence. While dark streaks in between metallic objects are often hard to reduce, reconstruction with patches seems to achieve this quite easily. This accelerated convergence is due to the sequential update of the patches and due to the smaller field of view of the smaller patches, which enables a bigger update step for these patches in each iteration [10]. This is also shown in the convergence experiment (figure 3 and 4) where we used 9 and 25 equally sized patches during the reconstruction. When comparing the reconstructions in figure 3 we see that the quality of the reconstruction improves by increasing the number of patches, for the same number of iterations. This indicates an improved overall convergence. This is also shown in figure 4 where we compare ΔL for the three reconstructions. ΔL decreases when more patches are used. We have seen a similar acceleration for other iterative reconstruction models, e.g. the convex algorithm [16].

Besides varying the resolution for the patches we also changed the projection model. In this way we limit the complex computation of IMPACT to a smaller area. As can be seen in figure 2(d) and 2(g), combining MLTR without water correction with IMPACT does not sufficiently reduce the artifacts, therefore we used a water corrected version of MLTR: MLTR_C. We see that the combination of IMPACT and MLTR_C (figure 2(g)) gives similar image quality as IMPACT for all patches (figure 2(f)). Using MLTR_C instead of IMPACT is considerably faster by using only 3 (back)projections per iteration instead of 8 for IMPACT.

In the future we want to apply this method to data coming from a clinical CT equipment. These data are often already precorrected for beam hardening effects in waterlike materials. We hope that the use of MLTR instead of MLTR_C will suffice for these data.

A possible disadvantage of the use of patches is that due to a different convergence between them, their edges can be visible. These edges often disappear by doing more iterations. Besides, the presence of these edges does probably not affect the clinical value.

In this study we have manually determined the location of the patches. This process could be automated by segmenting an initial raw FBP reconstruction and searching for the highly attenuating parts in the object by thresholding.

The presented patchwork approach also enables focus of attention reconstruction, where a particular region of interest is reconstructed with optimal parameters (increased resolution, full polychromatic modeling), while the rest of the object is reconstructed with reduced accuracy, ensuring high image quality where needed, obtained within an acceptable computation time. This would be particularly useful for in vivo microCT imaging, where often a relatively large field of view must be scanned for studying a small region of interest.

In a next step we will extent this patchwork reconstruction structure to three dimensions.

VI. Conclusion

The reduction of metal artifacts asks for an accurate, complex, often time consuming modeling of the acquisition. We

presented a structure, the patchwork projection, which makes use of local models and can in this way limit these complex calculations to certain subareas, patches, of the reconstruction volume. We could achieve similar image quality for a combined IMPACT/MLTR_C reconstruction, compared to a full IMPACT reconstruction. This reduced the complexity of the model for a major part of the reconstruction volume from 8 (back)projections to 3. Partial volume artifacts could be reduced by locally increasing the resolution which has only a minor influence on the computation time compared to an increased resolution for the whole image. Furthermore, the use of patches increases convergence which also eliminates persistent streaks in between metallic objects.

REFERENCES

[1] Barrett J. F. and Keat N., "Artifacts in CT: Recognition and avoidance.", *RadioGraphics*, 2004; 24:1679-1691.

[2] Zbijewski W. and Beekman F.J., "Characterization and suppression of the edge and aliasing artefacts in iterative x-ray CT reconstruction.", *Phys. Med. Biol.*, 2004; 49:145-157.

[3] De Man B. et al, "Iterative maximum-likelihood polychomatic algorithm for CT.", *Trans. Med. Im.*, 1995; 14 (1):132-137.

[4] Elbakri I. and Fessler J., "Statistical images reconstruction for polyenergetic x-ray computed tomography." *IEEE Trans Med Imaging*, 2002; 21 (2): 89-99.

[5] Menvielle N. et al., "Reduction of beam-hardening artifacts in x-ray CT.", *IEEE EMB Conference Prodeedings*, Shanghai, China, 2005.

[6] Glover G. and Pelc N., "An algorithm for the reduction of metal clip artifacts in CT reconstructions.", *Med. Phys.*, 1981; 8 (6): 799-807.

[7] Kalender W. et al. "Reduction of CT artifacts caused by metallic impants.", *Radiology*, 1987; 164: 567-568.

[8] Lemmens C., Faul D. and Nuyts J., "Suppression of metal artifacts in CT using a reconstruction procedure that combines MAP and projection completion.", *IEEE Trans Med Imaging*, 2009; 28 (2): 250-260.

[9] De Man B. and Basu S., "Distance-driven projection and backprojection in three dimensions.", *Phys. Med. Biol.*, 2004; 49: 2463-2475.

[10] Fessler J.A. et al, "Grouped-coordinate ascent algorithm for penalized-likelihood transmission image reconstruction.", *Trans. Med. Im.*, 1997; 16 (2): 166-175.

[11] Nuyts J. et al, "Iterative reconstruction for helical CT: a simulation study.", *Phys. Med. Biol.*, 1998; 43: 729-737.

[12] Meng L. J. and Li N., "Non-uniform object-space pixelation (NUOP) for penalized maxiumum-likelihood image reconstruction for a single photon emission microscope system.", *Trans. Nucl. Sci.*, 2009; 56 (5): 2777-2788.

[13] Maltz J. S., "Optimal time-activity basis selection for exponential spectral analysis: application to the solution of large dynamic emisson tomographic reconstruction problems.", *Trans. Nucl. Sc.*, 2001; 49 (4): 1452-1464.

[14] Brankov J.G. et al, "Tomographic image reconstuction using content-adaptive mesh modeling.", *Proc IEE Intl. Conf. on Image Processing*; 2001.

[15] De Man B. et al, "Metal streak artifacts in X-ray computed tomography: a simulation study.", *Trans. Nucl. Sci.*, 1999; 46 (3):691-696.

[16] Lange K. and Fessler J.,"Globally convergent algorithms for maximum a posteriori transmission tomography.", *Trans. Im. Pro.*, 1995; 4 (10): 1430-1438